Aeroacoustic Source Mechanisms in High-Speed Jets

Michael Crawley[1], Lior Gefen[2], Ching-Wen Kuo[3], Mo Samimy[3]† and Roberto Camussi[2]

[1]Department of Chemical Engineering, University of America, Somewhere, IN 12345, USA

[2]Department of Aerospace and Mechanical Engineering, University of Camford, Academic Street, Camford CF3 5QL, UK

[3]Department of Aerospace and Mechanical Engineering, University of Camford, Academic Street, Camford CF3 5QL, UK

Key words:

---

† Email address for correspondence: Samimy.1@osu.edu

1. Introduction

The advent of the turbojet engine led to a transformation in both commercial and military aviation, allowing for much faster flight than previously possible with propeller-driven aircraft. However, the increased thrust of turbojets has come at great cost; significant acoustic radiation is generated by the rotating components (compressor, turbine, fan), by the combustion process, and ultimately by the free jet itself. This has spurred extensive research, spanning over six decades, into the acoustic source mechanism in high speed, high Reynolds number jets. While progress has been made in the field of aeroacoustics, both experimentally (Tam *et al.* 1996; Viswanathan 2006; Tam *et al.* 2008) as well as theoretically (Cabana *et al.* 2008), understanding of jet noise sources and their radiation mechanisms remains incomplete (Jordan & Gervais 2008). This is due to the large number of interrelated parameters (e.g. Reynolds number, temperature ratio, acoustic Mach number, nozzle geometry, et cetera) as well as the large disparity in the associated length and time scales of the turbulent phenomena and the radiated noise. As a result, current noise-mitigation technologies for free jets have largely been applied in an ad hoc manner, due to the community's incomplete understanding of the aeroacoustic sources. Fully realizing this maximum noise reduction potential will require a much more detailed understanding of the mechanism (or mechanisms) by which free jets radiate to the far-field.

It is generally agreed that the dominant noise sources are related to the large-scale turbulent structures present in the mixing layer of the jet. As discussed by Tam (1995) (among many others), large-scale structures can be represented as instability waves superimposed upon the mean flow. At subsonic convection velocities, a plane instability wave with fixed frequency-wavenumber will emit no acoustic radiation to the far-field. However, modulation of the instability wave's amplitude creates a dispersion in the energy content of the instability wave. By doing so, the broadband instability wave, now commonly referred to as a *wavepacket*, can shift energy to supersonic phase-velocities and hence produce sound. Wavepacket models for noise emission have become commonplace, owing to their great success at predicting low-angle acoustic emission (Obrist 2011). Simple linear wavepacket models have allowed researchers to probe different aspects of the waveform modulation, in turn illuminating possible relevant dynamical behavior of the large-scale structures for the noise generation process. Temporal modulation of the wavepacket's amplitude and spatial extent ('jittering') were shown to increase the efficiency of the noise source (Cavalieri *et al.* 2011); this conforms to experimental results which have indicated that the noise generation in free jets is highly intermittent (Hileman *et al.* 2005; Kearney-Fischer *et al.* 2013). Though progress has been made in experimentally measuring wavepacket characteristics in high-speed turbulent jets (Cavalieri *et al.* 2013; Baqui *et al.* 2014), a direct link between large-scale structure dynamics and the aeroacoustic source has remained elusive.

The purpose of this work is to examine the dynamical evolutions of the large-scale coherent structures which lead to the dominant mixing noise in the subsonic, turbulent jet. The focus will be on the axisymmetric, toroidal vortices (azimuthal Fourier mode zero), as these are known to dominant the acoustic far-field. The jet will therefore be excited using localized arc-filament plasma actuators in order to generate these axisymmetric structures with a well-defined temporal frequency and phase. The irrotational near-field pressure will be acquired via a linear array of microphones, and decomposed into its constitutive acoustic and hydrodynamic components in order to identify the dominant noise source region. Time-resolved velocity fields will then be estimated based on stochastic correlations between the near-field pressure and the orthogonal modes of

ensemble (non-time-resolved) velocity field, identified by an artificial neural network. From these time resolved fields, the coherent structure dynamics will be identified. Lastly, the aeroacoustic source field will be computed using Ribner's Dilatation acoustic analogy (Ribner 1962). In doing so, the structure dynamics will be directly linked first to the acoustic source region, and finally to the acoustic sources themselves.

2. Experimental Methodology

All experiments were conducted at the Gas Dynamics and Turbulence Laboratory's anechoic chamber, details of which can be found in Hahn (2011). Compressed, dried, and filtered air is supplied to the facility from two cylindrical storage tanks with a total capacity of 43 m^3 and maximum storage pressure of 16 MPa. The air may be routed through a storage heater, which allows the jet to operate with a stagnation temperature up to 500 °C, before expanding through a nozzle and exhausting horizontally into an anechoic chamber. As the current work was focused on a cold jet, the heater was rarely necessary; in certain circumstances though (namely, long experimental runs) the storage heater and bandheaters were used to slightly preheat the flow, thereby mitigating the temperature drop as the storage tanks were drained of high-pressure air. Opposite the nozzle, a collector accumulates the jet and exhausts to the outdoors. The dimensions of the chamber are 6.20 m wide by 5.59 m long and 3.36 m tall, with internal wedge-tip to wedge-tip dimensions of 5.14 m by 4.48 m and 2.53 m, respectively. The design of the chamber produces a cutoff frequency of 160 Hz, below the frequencies of interest for this study.

For this study a converging, axisymmetric nozzle with exit diameter D of 25.4 mm was used. The nozzle utilized a thick-lipped design in order to simplify the mounts for the LAFPA extension, which housed the eight actuators used in this study. For the experiments reported in this paper, the jet was operated at a Mach number (M_j) of 0.90, and with a total temperature ratio of approximately unity. The Reynolds number based on the jet exit diameter was 6.2×10^5; previous investigations using hot-wire anemometry have indicated that the initial shear layer is turbulent for this operating condition with momentum thickness 0.09 mm and boundary layer thickness ~ 1 mm (Kearney-Fischer *et al.* 2009).

2.1. *Localized Arc-Filament Plasma Actuators*

The design of the localized arc-filament plasma actuators, as well as the driving circuitry, has undergone a slow evolution since their initial development by the GDTL and NETL. In the current work, each LAFPA actuator consists of a pair of 1 mm diameter tungsten pin electrodes. The center-to-center spacing between electrode pairs for each actuator is 4 mm. Eight actuators were uniformly spaced around the nozzle perimeter 1 mm upstream of the nozzle exit. For electrical and thermal durability, the electrodes were housed in a boron nitride extension attached to the end of the nozzle. A groove with dimensions of 1 mm wide and 0.5 mm deep is machined in the boron nitride, into which the electrode tips protrude; this provides a region of low momentum flow in order to stabilize the plasma arcs. It has been shown that the existence of this groove does not substantially alter the flow field or the control authority of the LAFPAs (Hahn *et al.* 2011). A detailed description of initial development and LAFPA characteristics can be found in Utkin *et al.* (2007).

The LAFPAs were energized by a multi-channel, high-voltage plasma power generator capable of simultaneously powering up to eight LAFPAs, which was designed and built in-house at the GDTL. In this second-generation power supply, each individual circuit consists of a switchable capacitor in line with a high voltage transformer; the arcing electrodes are connected to the secondary side of the coil. The capacitor is charged by a 100 V DC power supply when the first switch is closed and the second is opened; at the user-specified time the switches flip and it discharges through the coil. The switches are controlled by a 16-channel digital I/O card and National Instruments' Labview software, operated by a dedicated computer. The plasma generator provides independent control

of the frequency, duty cycle/pulse width, and phase of each individual actuator (though not the amplitude). The pulse width was held constant at 7 s, which was found to be the minimum pulse width at which the actuators consistently arced for all frequencies explored in this study (Hahn *et al.* 2011). The circuit is limited to 20 kHz due to thermal concerns. However, as the current work is focused on the evolution of large-scale structures (and ultimately their acoustic radiation), for which the dominant frequencies are on the order of 3 kHz, this is not an issue.

2.2. *Time-Resolved Pressure*

Near-field and far-field pressure measurements were acquired using Brüel & Kjær 0.25-inch 4939 microphones and preamplifiers. The signal from each microphone is band-pass filtered from 20 Hz to 100 kHz using a Brüel & Kjær Nexus 2690 conditioning amplifier, and recorded using National Instruments PXI-6133 A/D boards and LabVIEW software. The microphones are calibrated using a Brüel & Kjær 114 dB, 1 kHz sine wave generator (type 4231). The frequency response of the microphones is flat up to roughly 80 kHz, with the protective grid covers removed.

Far-field acoustic pressure is acquired at three polar angles: 30°, 60° and 90°, as measured from the downstream jet axis. The microphones were oriented such that they are at normal incidence to the jet downstream axis at the nozzle exit. The radial distance of the microphones ranges from $101D$ at 30° to $145D$ at 60°.

The near-field pressure was acquired during two separate experimental campaigns; the first focusing purely on the near-field and far-field pressure and the second focusing on the instantaneous velocity field. During the first campaign, the irrotational near-field was acquired using a linear array of sixteen microphones located along the meridional plane of the jet; the spacing varied along the array from $1D$ to $2D$. The array was inclined at an angle of 8.6° to the jet axis in order to match the spreading angle of the jet shear layer, as determined via PIV measurements during previous studies (Kearney-Fischer *et al.* 2009). Voltage signals were collected at 200 kHz with 81920 data points per block; sub-blocks of 8192 data points were used when calculating short-time power spectral densities, resulting in a frequency resolution of 24.4 Hz. Ten blocks were recorded for each case resulting in four seconds of data, which has been found to be sufficient for statistical convergence.

In the second experimental campaign, a shorter array consisting of 12 microphones equally spaced by $1D$ was used. In this case, the array was mounted from the floor and at an angle off the meridional plane of the jet (with microphone tips angled normal to the jet axis). This setup was used in conjunction with the particle image velocimetry described in the following section; the microphone array was placed off of the meridional plane so that it did not intersect with the laser sheet. As before, the microphone array was angled 8.6° with respect to the jet axis in order to match the spreading rate of the shear layer, and the axial and radial positions were set to match the closest microphone array location used during the first experimental campaign. Voltage traces were acquired at 400 kHz, with 24576 points collected per block. The voltage traces were collected simultaneously with streamwise particle image velocimetry measurements; 1500 blocks were acquired, corresponding to the 1500 acquired images.

In addition to the microphone voltage traces, the acoustics data acquisition system recorded a reference signal corresponding to the LAFPA excitation. The TTL pulse sequence, which controls the LAFPAs, was supplied to an Agilent 3320A waveform generator. The rising edge of the TTL pulse triggered a sharp drop in the output voltage of the waveform generator, which then ramps back up to the original voltage over a time interval which is shorter than the minimum excitation period. The output from the

waveform generator was acquired simultaneously with the near- and far-field pressure signals using the aforementioned National Instruments hardware and software. As the excitation frequency, azimuthal mode, and ramp signal are well defined, this system enables the identification of the zero phase of actuation and hence, the ability to phase-average the pressure signals over the excitation period, akin to the work performed in Sinha *et al.* (2012).

2.3. *Snapshot Particle Image Velocimetry*

The instantaneous velocity was acquired using streamwise, two-component particle image velocimetry (PIV). A Spectra Physics, double-pulsed Nd:YAG laser (model PIV-400) was used as the illumination source. Due to facility requirements, the laser was located on a vibrationally-damped table outside the anechoic chamber and the laser beam was routed into the chamber using an overhead port; this resulted in a beampath of ~10 m. The laser sheet was formed using two cylindrical and one spherical lens; one of the cylindrical lenses was mounted to a rotational stage in order to ensure that the final laser sheet was normal to the jet exit. Alignment of the separate laser heads was initially performed using burn paper; final alignment was performed by seeding a low-velocity flow and visually checking that the same particles were captured in both frames. Per the best practices explained in the LaVision DaVis manual, the timing between the two laser pulses was set so that particles in the jet core translated downstream by roughly half of the minimum correlation window width (16 pixels). For the present work, this resulted in a time delay of 3 μs. It was later observed that the actual time delay produced by the laser did not match the delay specified in the control software; this resulted in incorrect velocities being computed by the cross-correlations. In order to correct for this, the laser pulses were recorded using a ThorLabs DET210 photodetector and a LeCroy Wavejet 324A oscilloscope; the final vector fields were linearly scaled based on the ratio between the specified time delay and the measured time delay.

The jet core was seeded using Di-Ethyl-Hexyl-Sebacat (DEHS); the oil was atomized using a LaVision Aerosol generator and injected upstream of the turbulence screens in the stagnation chamber in order to produce a uniform seed particle density. As the jet entrains a significant amount of the surrounding ambient fluid as it evolves downstream, the coflow around the jet must also be seeded in order to accurately measure the outer shear layer velocity. For this, a TSI 6-jet atomizer and olive oil was used; injection occurred into a plenum which surrounded the core stagnation chamber. Per the manufacturer's specfications, both atomizers provided nominally sub-micron seed particles. To ensure consistent seeding, this coflow was driven using a small blower and a series of high-pressure ejectors. As a result, for the PIV data acquisitions, the jet core was surrounded by a ~5 m/s coflow.

Image groups were acquired using two LaVision Imager Pro SX 5M cameras, which had 12-bit resolution and 2560×2180 pixels. The combination of the PIV-400 laser and the Imager Pro SX cameras resulted in a maximum acquisition rate for the image groups of 5 Hz. The cameras were positioned such that they were nominally normal to the image plane, negating the need for scheimpflug mounts. This was done as having high spatial resolution and field of view were deemed to be more important than having full, three-component velocity vectors. The cameras were aligned such that there was roughly a 10% overlap between the two images. This setup is generally designated as "side-to-side" in order to differentiate it from stereoscopic PIV; a schematic of the setup can be found in Fig. 1.

The image groups were acquired randomly in time at the system's maximum acquisition rate (5 Hz). The PIV computer was set to output a reference signal which was
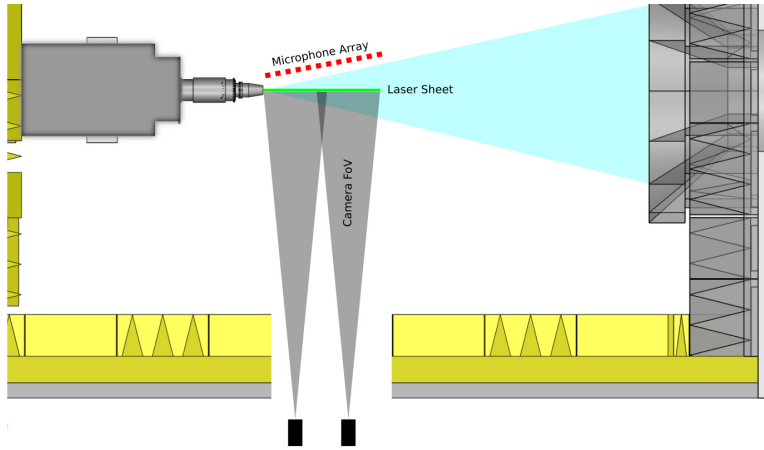
Figure 1: Schematic of syncronized PIV and near-field pressure data acquisition setup.

used to trigger the acoustics data acquisition system. The timing was set such that the PIV image acquisition would occur roughly in the center of a data block acquired by the acoustics system; the signal from a photoreceiver was also recorded in order to accurately identify the timing of the image acquisition in relation to the pressure time traces. For this case, 1500 image groups were acquired for each case.

3. Vortex Dynamics in a Turbulent Mixing Layer

Analysis of the evolution, interaction, and disintegration of the large-scale structures, and ultimately the noise generated thereby, is greatly simplified by the acquisition of time-resolved flow-field measurements. Furthermore, as will be explained in §4, computation of the aeroacoustic source field from a simplified acoustic analogy will require time-resolved flow-field data. Unfortunately, directly acquiring time-resolved velocity fields for the jet currently under study is simply not possible due to the combination of a large domain of interest ($0 \leqslant x/D \lesssim 12, 0 \leqslant r/D \lesssim 3$) and high characteristic frequencies on the order of tens of kHz. Full-field, high-fidelity measurement techniques capable of this required repetition rate simply do not exist at present. An indirect method is therefore required in order to estimate the evolution of the large-scale structures, in a reduced-order sense.

Phase-locking of a data acquisition system to a reference signal (such as an actuator or a naturally occurring resonance tone) is a common experimental technique, and was initially considered for the present work. However, sample analysis performed using a numerical database indicated that a very high temporal resolution was required in order to accurately compute fluctuation rates in the dilatation field (the relevance of which will become more apparent in the following section). At moderate to high excitation frequencies, this was feasible, though potentially tedious (for example, $\sim$16 phases were estimated as necessary at $St_{DF} = 0.25$). At $St_{DF} = 0.05$ however, this would require roughly *forty* phases (the significant dead time between actuations means that it is not necessary to acquire the entire range of phases from 0 to 2π, but this is small consolation). Clearly, a more efficient data acquisition method is needed.

3.1. *Stochastic Estimation*

The current work borrows heavily from the methodology of Tinney *et al.* (2008) and Sinha *et al.* (2010) in order to estimate the two-component time-resolved velocity field on a streamwise slice of the jet. The computational methodology by which the stochastic estimation is performed has been modified, however. Complementary stochastic estimation is used, due to its significantly lower computational cost as well as theorized improvement in accuracy (Bonnet *et al.* 1994). The estimated velocity fields produced by LSE were projected onto the POD eigenfunctions (computed from the random, non-time-resolved velocity fields) to produce an estimate of the time-dependent POD coefficients, which can then be used to reconstruct low-order representations of the estimated random velocity field. Multiple time delays are incorporated, as this has been found to significantly improve the accuracy of the reconstructions for many flow regimes (Ewing & Citriniti 1997; Tinney *et al.* 2006, 2008; Durgesh & Naughton 2010). Instead of performing the stochastic estimation using either linear or higher-order cross-correlations (or cross-spectra), the conditional mapping between the near-field pressure and the POD modal coefficients will be generated by an artificial neural network (ANN). ANNs were chosen over the more traditional cross-correlations due to their simplicity compared to high-order methods as well as their demonstrated ability to model nonlinear processes in turbulent flows (Lasagna *et al.* 2015).

A feedforward network structure was used in the current work; comprised of an input layer, to which near-field pressure traces were supplied, a single hidden layer containing 32 neurons, and an output layer which produced estimates of the time-varying POD coefficients. The hidden and output layers were fully connected, and the modified logistic function (hyperbolic tangent) was used as the activation function. The pressure traces were centered around the acquisition of a PIV image group, and was downsampled to 100 kHz in order to approximate the frequency response of the microphones. The record

time supplied for each training block was ± 2.56 milliseconds; this was determined by estimating the time delay for a large-scale structure to convect through the experimental domain (the convective velocity of the large-scale structures was conservatively estimated as $U_c \simeq 0.5 U_j$).

POD modes and time-varying coefficients were computed from the velocity fields using the method of snapshots (Sirovich 1987); the kernel was defined as the two-component turbulent kinetic energy. The instantaneous velocity fields were not preprocessed prior to the decomposition (that is, missing or spurious vectors were not replaced or interpolated). As experimental noise in the velocity fields will be completely uncorrelated to the near-field measurements, it will be filtered out by the stochastic estimation and hence preprocessing is unnecessary. In this work, the coefficients for every POD mode were estimated, rather than just the most energetic modes, for two reasons. First, it is not guaranteed that an individual POD mode corresponds to a physically distinct turbulent flow structure or event - an event may be broken up into multiple POD modes of varying energy levels. Secondly, the most energetic POD mode is not necessarily the most relevant mode for the acoustic generation process (see Jordan *et al.* (2007) for a modification to the standard POD kernel in order to mitigate this issue). The second issue is in fact not unique to the field of aeroacoustics but vexes turbulence research in general, where highly relevant dynamical processes may contain little energy (Noack *et al.* 2008); this has lead researchers to propose alternative methods for extracting dynamical features of turbulent flows (Schmid 2010). Even though the network is estimating even the least-energetic modes, the current method is far more computationally efficient than directly estimating the velocity fields themselves. By encoding spatial correlations in the POD expansion coefficients, estimation of the N snapshots of $M \times K$ spatial locations has been reduced from a minimization problem of N vectors of $2MK$ to one of N vectors of N. For the current experimental database, this means the system has been reduced from $290,508 \times 1500$ to 1500×1500. The neural network now only needs to identify the temporal correlations between the pressure field and the individual POD coefficients; it does not need to learn the spatial correlations.

Learning was accomplished via the standard backpropagation method (Haykin 1994), which approximates the error surface of the cost function using first-order derivatives; the error 'propagates' backwards from the output neurons to the hidden neurons and the synaptic weights at each neuron are updated to identify the (hopefully, global) minimum of the cost function using gradient descent. The cost function was defined as the mean-squared-error between the predicted and measured expansion coefficients for a given PIV image group. Training of the network was performed using the roughly 1500 ensemble pressure-velocity blocks of data (a few PIV images in each set had to be discarded due to laser misfires); synaptic weights were updated based on the average of all blocks (batch processing) using a constant learning rate. A well-known issue with the gradient descent optimization method is that it has a tendency to get trapped in local minima and fails to converge to the global minimum. Therefore, sample results were also calculated using a much different learning algorithm: adaptive particle swarm optimization. Details will not be presented here however, as the results were found to not differ substantially from those produced by the backpropagation algorithm (while requiring significantly higher computational resources).

4. The Aeroacoustic Source Field

REFERENCES

BAQUI, Y. B., AGARWAL, A. & CAVALIERI, A. 2014 A coherence-matched linear model for subsonic jet noise. In *20th AIAA/CEAS Aeroacoustics Conference*.

BERKOOZ, G., HOLMES, P. & LUMLEY, J. L. 1993 The proper orthogonal decomposition in the analysis of turbulent flows. *Annual Review of Fluid Mechanics* **25**, 539–575.

BONNET, J.-P., COLE, D. R., DELVILLE, J., GLAUSER, M. N. & UKEILEY, L. S. 1994 Stochastic estimation and proper orthogonal decomposition: Complementary techniques for identifying structure. *Experiments in Fluids* **17** (5), 307–314.

CABANA, M., FORTUNÉ, V. & JORDAN, P. 2008 Identifying the radiating core of lighthill's source term. *Theoretical Computational Fluid Dynamics* **22**, 87–106.

CAVALIERI, A., JORDAN, P., AGARWAL, A. & GERVAIS, Y. 2011 Jittering wave-packet models for subsonic jet noise. *Journal of Sound and Vibration* **330**, 4474–4492.

CAVALIERI, A., RODRIGUEZL, D., JORDAN, P., COLONIUS, T. & GERVAIS, Y. 2013 Wavepackets in the velocity field of turbulent jets. *Journal of Fluid Mechanics* **730**, 559–592.

DURGESH, V. & NAUGHTON, J. W. 2010 Multi-time-delay lse-pod complementary approach applied to unsteady high-reynolds-number near wake flow. *Experiments in Fluids* **49** (3), 571–583.

EWING, D. & CITRINITI, J. H. 1997 Examination of a lse/pod complementary technique using single and multi-time information in the axisymmetric shear layer. In *Proceedings of the IUTAM Symposium on simulation and identication of organized structures in flows* (ed. J.N. Sorensen, E.J. Hopfinger & N. Aubry), pp. 375–384. Lyngby, Denmark: Kluwer Academic Press.

HAHN, C. 2011 Design and validation of the new jet facility and anechoic chamber. Masters, The Ohio State University.

HAHN, C., KEARNEY-FISCHER, M. & SAMIMY, M. 2011 On factors influencing arc filament plasma actuator performance in control of high speed jets. *Experiments in Fluids* **51** (6), 1591–1603.

HAYKIN, S. 1994 *Neural Networks A Comprehensive Foundation*. Macmillan College Publishing Company.

HILEMAN, J., THUROW, B., CARABALLO, E. J. & SAMIMY, M. 2005 Large-scale structure evolution and sound emission in high-speed jets: real-time visualization with simultaneous acoustic measurements. *Journal of Fluid Mechanics* **544**, 277–307.

JORDAN, P. & GERVAIS, Y. 2008 Subsonic jet aeroacoustics: associating experiment, modelling and simulations. *Experiments in Fluids* **44**, 1–21.

JORDAN, P., SCHLEGEL, M., STALNOV, O., NOACK, B.R. & TINNEY, C.E. 2007 Identifying noisy and quiet modes in a jet. In *13th AIAA/CEAS Aeroacoustics Conference (28th AIAA Aeroacoustics Conference)*, , vol. Paper 2007-3602.

KEARNEY-FISCHER, M., KIM, J.-H. & SAMIMY, M. 2009 Control of a high reynolds number mach 0.9 heated jet using plasma actuators. *Physics of Fluids* **21**, 095101.

KEARNEY-FISCHER, M., SINHA, A. & SAMIMY, M. 2013 Intermittent nature of subsonic jet noise. *AIAA Journal* **51** (5), 1142–1155.

LASAGNA, D., FRONGES, L., ORAZI, M. & IUSO, G. 2015 Nonlinear multi-time-delay stochastic estimation: Application to cavity flow and turbulent channel flow. *AIAA Journal* **53** (10), 2920–2935.

NOACK, B. R., AFANASIEV, K., MORZYNSKI, M., TADMOR, G. & THIELE, F. 2008 A hierarchy of low-dimensional models for the transient and post-transient cylinder wake. *Journal of Flui* **497**, 103–148.

OBRIST, D. 2011 Acoustic emissions from convected wave packets. *Physics of Fluids* **23**, 026101.

RIBNER, H. S. 1962 Aerodynamic sound from fluid dilatations. UTIA Report 86. Institute of Aerophysics, University of Toronto.

SCHMID, P. 2010 Dynamic mode decomposition of numerical and experimental data. *Journal of Fluid Mechanics* **656**, 5–28.

SINHA, A., ALKANDRY, H., KEARNEY-FISCHER, M., SAMIMY, M. & COLONIUS, T. 2012 The impulse response of a high-speed jet forced with localized arc filament plasma actuators. *Physics of Fluids* **24**, 125104.

SINHA, A., SERRANI, A. & SAMIMY, M. 2010 Initial development of reduced-order models for feedback control of axisymmetric jets. *International Journal of Flow Control* **2** (1), 39–60.

Sirovich, L. 1987 Turbulence and the dynamics of coherent structures, parts i-iii. *Quarterly of Applied Mathematics* **XLV** (3), 561–590.

Tam, C. K. W. 1995 Supersonic jet noise. *Annual Review of Fluid Mechanics* **27**, 17–43.

Tam, C. K. W., Golebiowski, M. & Seiner, J. M. 1996 On the two components of turbulent mixing noise from supersonic jets. In *2nd AIAA/CEAS Aeroacoustics Conference*.

Tam, C. K. W., Viswanathan, K., Ahuja, K. & Panda, J. 2008 The source of jet noise: Experimental evidence. *Journal of Fluid Mechanics* **615**, 253–292.

Tinney, C. E., Coiffet, F., Delville, J., Hall, A. M., Jordan, P. & Glauser, M. N. 2006 On spectral linear stochastic estimation. *Experiments in Fluids* **41**, 763–775.

Tinney, C. E., Eukeiley, L. S. & Glauser, M. N. 2008 Low-dimensional characteristics of a transonic jet. part 2. estimate and far-field prediction. *Journal of Fluid Mechanics* **615**, 53–92.

Utkin, Y., Keshav, S., Kim, J.-H., Kastner, J., Adamovich, I. & Samimy, M. 2007 Development and use of localized arc filament plasma actuators for high-speed flow control. *Journal of Physics D: Applied Physics* **40** (3), 685–694.

Viswanathan, K. 2006 Scaling laws and a method for identifying components of jet noise. *AIAA Journal* **44** (10), 2274–2285.